

Stochastic Heating of a Bose-Einstein Condensate

Xiao-Qiong Wang,¹ Rui-Lang Zeng,¹ Zi-Yao Zhang,¹ Chushun Tian,²
Shizhong Zhang,³ Andreas Hemmerich,⁴ and Zhi-Fang Xu^{1,*}

¹*Shenzhen Institute for Quantum Science and Engineering and Department of Physics,
Southern University of Science and Technology, Shenzhen 518055, China*

²*CAS Key Laboratory of Theoretical Physics and Institute of Theoretical Physics,
Chinese Academy of Sciences, Beijing 100190, China*

³*Department of Physics and Hong Kong Institute of Quantum Science and Technology,
The University of Hong Kong, Hong Kong, China*

⁴*Institute of Quantum Physics, University of Hamburg,
Luruper Chaussee 149, 22761 Hamburg, Germany*

Understanding and controlling non-equilibrium processes at ultralow temperatures are central to quantum physics and technology. In such extreme environments, quantum coherence and dissipation can interact intimately to give rise to intriguing thermalization phenomena. Here, we experimentally and theoretically demonstrate a novel scenario of thermalization in an ultracold atomic system, distinct from various quantum thermalization scenarios currently under intense investigations. We observe that after a sudden quench, an atomic Bose-Einstein condensate (BEC) behaves as a rigid body and undergoes a random walk in momentum space due to atom loss and interactions with the surrounding thermal component. Consequently its center of mass degree of freedom gets heated up at a constant rate. This heating mechanism, rooted in random momentum scattering, falls into the paradigm of stochastic heating initiated by Fermi and thoroughly explored in plasma physics, which differs conceptually from the traditional thermal conduction. At longer times, the stochastic heating of the BEC is balanced by forced evaporative cooling, and a Maxwell-Boltzmann distribution is achieved. Our findings offer new perspectives on the non-equilibrium dynamics of open Bose systems at ultralow temperature and quantum thermalization.

Quantum properties such as matter wave coherence and interference can strongly influence particle motion, leading to a multitude of unconventional non-equilibrium processes [1–4]. In-depth exploration of this topic advances our understanding of statistical mechanics and provides guiding principles for quantum technology. Owing to their high degree of control and tunability, ultracold atomic systems provide a unique platform for pursuing this task. A broad range of non-equilibrium phenomena, such as quantum Newton’s cradle [5], many-body localization [6, 7], quantum thermalization [8], dynamical scaling [9, 10], quantum turbulence [11] and dynamical localization [12–16], have been observed experimentally. The primary focus has been on closed systems, with growing interest in open and dissipative systems. In cold atom experiments, openness and dissipation, notably arising from atom loss, are ubiquitous and crucial for cooling these systems to low temperatures required for the realization of exotic quantum phases.

For generic Bose systems, below a critical temperature, a coherent condensate develops and interacts with the incoherent thermal component, giving rise to rich dynamical phenomena. A canonical example is the coexistence of the first and second sound at low temperatures, well described by Landau’s two-fluid theory [17] and remaining at the heart of experiments on ultracold atomic systems [18–23]. Yet, these two kinds of sound are near-to-equilibrium phenomena in closed systems. Non-equilibrium dynamics of open condensate systems, with an emphasis on interactions between coherent and in-

coherent components, provide an interesting yet rarely explored new frontier in cold atom physics.

Despite its quantum nature, a Bose-Einstein condensate (BEC) with regard to its center-of-mass coordinate (COM) can behave as a macroscopic classical object. A multitude of studies have addressed the internal dynamics of BECs, associated with its relative coordinates, such as collective excitations, while little attention has been paid to its COM dynamics. When the system is driven out of equilibrium, say, by a quantum quench, the interaction of the condensate with the surrounding thermal cloud can give rise to intricate condensate COM dynamics, whose properties and consequences have remained largely unexplored.

In this study, we carried out an experimental investigation of quench dynamics of a cloud of ⁸⁷Rb atoms in an optical lattice, and performed theoretical analysis to uncover a novel dynamical phenomenon displayed by the condensate COM. We find that, in the presence of atom loss, a sudden quench neither destroys the condensate nor leads to fragmentation; rather, the condensate as a whole and hence its COM undergoes random momentum scattering and displays a diffusive motion in the momentum space. As a consequence, while the condensate remains fully coherent, its COM attains kinetic energy and gets heated up. This heating mechanism bears a firm analogy to the famous stochastic heating in plasma physics [24–27]. Eventually, when heating is balanced by forced evaporative cooling associated with atom loss, thermal equilibrium is established described by a Maxwell-Boltzmann

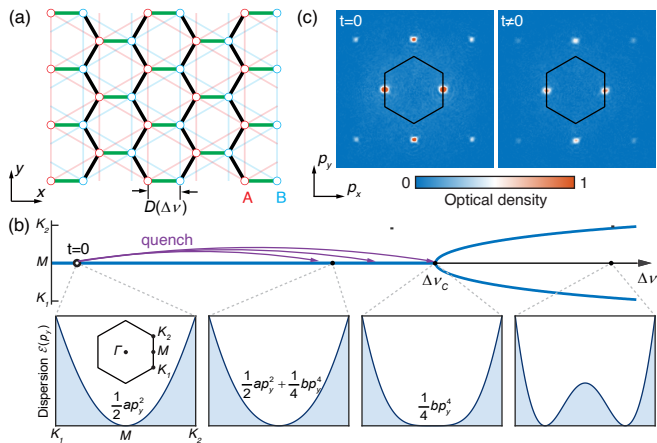


FIG. 1. Quench dynamics of BEC. (a) A hexagonal optical lattice, formed by superposing two triangular sub-lattices with lattice sites labeled as A and B, is deformed, characterized by the distance D between nearest A and B sites in the x -direction. D depends on the frequency difference $\Delta\nu$ between lasers for generating two sub-lattices. (b) The second-band dispersion evolves with $\Delta\nu$. For small $\Delta\nu$ a single minimum appears at the M point, while at a critical value $\Delta\nu_c$ it bifurcates into two minima located at the edges of the first Brillouin zone. At $t = 0$, a BEC is prepared with $\Delta\nu$ well below the critical point, and an almost quadratic dispersion results. The system is then suddenly quenched into the vicinity of the critical point, but not across it. (c) Both pre- and post-quench momentum distribution obtained from TOF measurements exhibit sharp Bragg peaks, indicating that strong coherence is maintained in the entire course of quench dynamics.

distribution.

Experimentally, we use an oblate dipole trap and a two-dimensional hexagonal optical lattice [28, 29] to confine atoms. The lattice potential is formed by superposing two triangular sub-lattices, with lattice sites labeled as A and B, respectively. Each sub-lattice is generated by interference of three laser beams, linearly polarized along the z -axis and propagating in the xy -plane with a wavelength $\simeq 1064$ nm. We adjust the frequency difference $\Delta\nu$ between two sets of laser beams to control the relative displacement between two sub-lattices, as illustrated in Fig. 1(a). This displacement, denoted as $D(\Delta\nu)$, represents the distance between nearest neighbor sites along the x -axis. Varying $\Delta\nu$ and the relative depth of the two triangular sub-lattices, we can finely tune the dispersion of the second Bloch band. In Fig. 1(b), we illustrate how the second-band dispersion around the M point transits in the p_y direction from a quadratic to quartic and eventually to double-well form, as $\Delta\nu$ increases and passes through a critical point $\Delta\nu_c$. The dispersion in the other two directions is always quadratic.

Initially, we load atoms into the second band and implement forced evaporative cooling to induce a BEC around the sole band minimum at M point, confirmed by time-of-flight (TOF) measurements depicted in Fig. 1(c),

where sharp Bragg peaks indicate strong coherence among atoms. We then study quench dynamics by suddenly changing $\Delta\nu$ to some value that approaches, but does not exceed $\Delta\nu_c$. This ensures that the M point remains the minimum of the excited band after the quench.

Upon the sudden quench, a certain amount of energy is injected into the system, driving it out of equilibrium. From previous works on closed systems, one might anticipate observing domain walls after the quench. Contrary to this expectation, our measurements indicate that the degree of coherence of the BEC remains high throughout the entire course of the experimental observations, as evidenced by sustained sharp Bragg peaks in TOF measurements (see Fig. 1(c) for example). We attribute this sustained coherence to forced evaporative cooling originating from interaction-induced atom loss along the gravity direction, as observed in previous experiments [28, 30]. Moreover, repeating experiments with the same evolution time t , we observe substantial fluctuations of the momentum distributions. In Fig. 2(a), we present the momentum distributions derived from TOF measurements at $t = 300$ ms after the system was quenched to $\Delta\nu = 3.23$ GHz, which is near the critical point. In each individual run, atoms condense around a specific momentum with a mean \mathbf{p}_c . Here, the subscript ‘ c ’ represents the average with respect to the single-run momentum distribution around two equivalent primarily occupied Bragg peaks on the boundary of the first Brillouin zone, connected by a reciprocal lattice vector. While the x -component of \mathbf{p}_c hardly changes for different experimental runs, we observed that its y -component $p_{c,y}$ strongly fluctuates, manifesting in significant deviations of the main Bragg peaks from the M points.

We perform consecutive experimental runs for more than 300 iterations for each evolution time, and record $p_{c,y}$, which are exemplified in Fig. 2(b). At time $t = 0$, the fluctuations of $p_{c,y}$ are very weak, suggesting that the initial preparation of the BEC is highly reproducible. As the time increases, fluctuations become stronger and the center of the main Bragg peak displays an increased random motion in the momentum $(p_{c,y})$ space. In the most significant instances, fluctuations drive the peak center from the M to the K_1 (or K_2) point at the corner of the first Brillouin zone. Furthermore, the histogram of measurements of $p_{c,y}$ is well fitted by a Gaussian distribution at each instant after the quench. In contrast, we find that $p_{c,x}$ does not exhibit significant fluctuations. This can also be seen from Fig. 2(a), where the main Bragg peaks stay at the K_1 - K_2 line throughout the experiment. To analyze fluctuations of $p_{c,y}$, we further compute the mean and variance denoted as $E[p_{c,y}]$ and $\text{Var}[p_{c,y}]$, respectively, with the average over repeated measurements at the same evolution time. The results are shown in Fig. 2(c) and (d). We observe that $E[p_{c,y}]$ remains small and exhibits damped oscillations over time. Moreover, $\text{Var}[p_{c,y}]$ increases with time, gradually reaching satu-

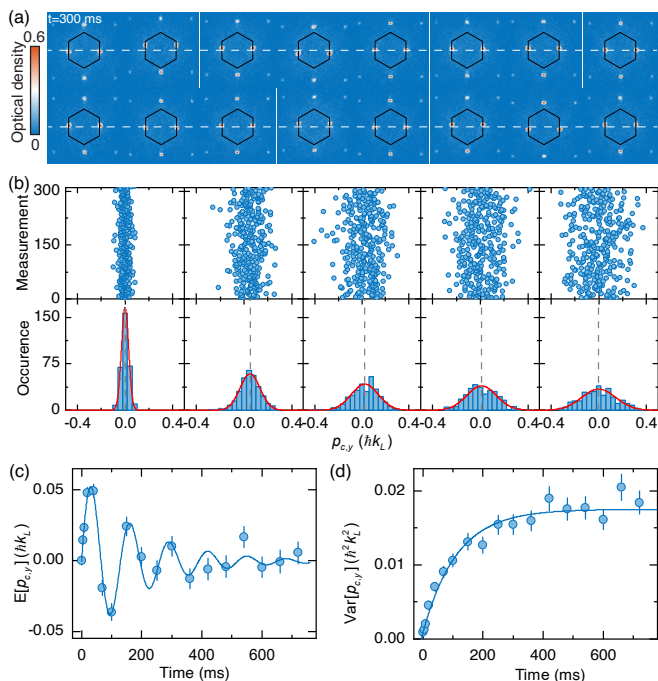


FIG. 2. Momentum fluctuations of BEC in quench dynamics. (a) We show the measured momentum distribution of the BEC at $t = 300$ ms after quench. Subfigures represent results from different experimental runs. They all reveal condensation around a single momentum, but clearly the momentum location displays strong fluctuations. Horizontal dashed lines correspond to $p_y = 0$. (b) The mean value of momentum $p_{c,y}$ for the BEC across different measurements at $t = 0, 40, 150, 300,$ and 660 ms, along with the corresponding histogram shown below. Red solid curves indicate Gaussian fitting and longitudinal dashed lines represent their center positions. (c) The temporal profile of $p_{c,y}$ averaging over 300 repeated measurements. (d) The temporal profile of the variance of $p_{c,y}$. Here, dots denote experimental data and the solid line denotes a fitting curve. Error bars represent the standard deviation.

ration after several hundred milliseconds of evolution. These observations imply that dissipation is essential to our system, and the random motion equilibrates at long time. Later on, we will develop a theoretical model that explains the experimental results quantitatively and uncovers their underlying mechanism.

To obtain additional insights into the random momentum fluctuations of the condensate, we conduct further experiments and quench the system with different strengths, such that $\Delta\nu$ takes different values below the critical point. Figure 3 summarizes our results. It shows that momentum fluctuations arise for all quench strengths. Clearly, as we bring the system closer to the critical point, the amplitude of the oscillation of $E[p_{c,y}]$ increases (Fig. 3(a)), and so does the oscillation period (Fig. 3(c)); simultaneously, the variance of $p_{c,y}$ increases more rapidly and reaches a higher saturation value denoted as S_V (Fig. 3(b) and (d)).

In order to distinguish the relative populations and

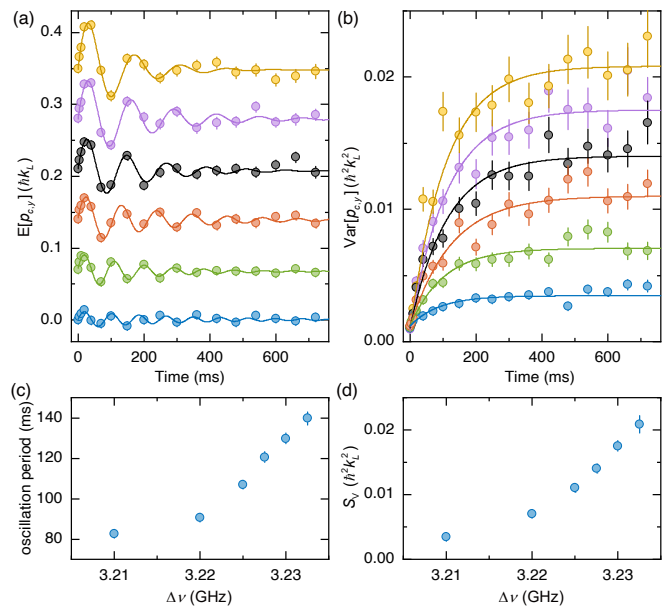


FIG. 3. Momentum fluctuations for different quench strengths. (a) Temporal profiles of the mean $p_{c,y}$ for different quench parameters: $\Delta\nu = 3.21, 3.22, 3.225, 3.2275, 3.23,$ and 3.2325 GHz from bottom to top. They are all close to, but do not exceed the critical value. The upper five data sets are shifted upwards to aid legibility. Dots represent experimental data and lines represent the fitting curve. (b) Temporal profiles of the variance of $p_{c,y}$ obtained from the same experimental data sets used in (a), plotted in the same color. Error bars represent the standard deviation. (c, d) Dependence of the oscillation period and the saturation value of variance on $\Delta\nu$. They are obtained by fitting experimental data.

band-specific distributions of the thermal and condensed fractions, we complement in Fig. 4 the TOF data obtained in Figs. 2 and 3 by means of a band-mapping technique [31], that enables the observation of the quasi-momentum distribution. In Fig. 4(a), we present quasi-momentum spectra at two different holding times $t = 0$ and $t = 300$ ms. Initially (at $t = 0$), atoms predominantly occupy the second Bloch band, with a significant fraction of atoms condensed around the M point, evidenced by sharp Bragg peaks. Assuming negligible coherence beyond nearest neighbors among thermal atoms, we approximate a uniform distribution for them in the second band via band mapping, facilitating separate counts of condensed and thermal atoms [32]. Figure 4(b) depicts the corresponding temporal evolution of the respective atom numbers. We observe that the loss of thermal atoms is faster than that of the condensed component, resulting in an increased fraction of condensed atoms in the second band, which saturates after several hundred milliseconds (Fig. 4(c)), indicating thermal equilibrium between thermal atoms and condensed atoms in the second band. Additionally, a notable population of atoms exists in the lowest Bloch band. Given our experimental param-

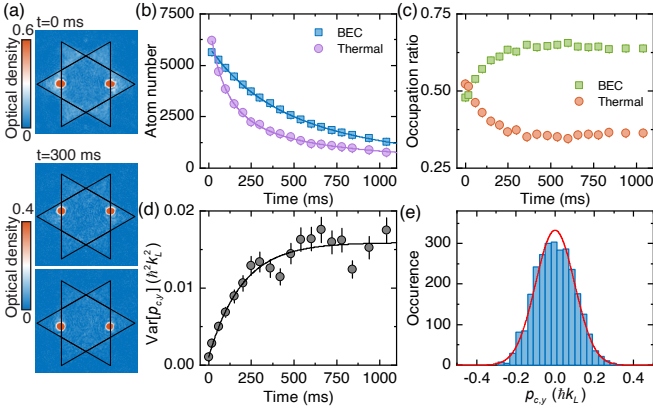


FIG. 4. Time evolution of condensed and thermal atoms. (a) Quasi-momentum distributions obtained from band-mapping measurements for $t = 0$ and $t = 300$ ms. For the latter case, two representative results are shown. The inner solid hexagon and the six surrounding triangles denote, respectively, the first and second Brillouin zones. (b) Time dependence of atom number for condensed (squares) and thermal parts (circles) in the second Bloch band. Solid lines represent corresponding fitting based on the one-body and two-body loss model. (c) Occupation ratios for condensed atoms and thermal atoms in the second band. (d) Time dependence of the variance of $p_{c,y}$ for the condensed atoms at $\Delta\nu = 3.2275$ GHz. Here, in calculating the mean value of momentum $p_{c,y}$, we take into account only the condensed atoms. (e) Histogram of $p_{c,y}$ at saturated regime with $t = 940$ ms. The corresponding Gaussian fitting is indicated by red solid curve.

eters, atoms in the first band primarily occupy s -orbitals of deeper lattice sites, spatially segregated from those in the second band, which mainly occupy s -orbitals of the shallower lattice sites. Due to minimal contact interaction between first and second band atoms, thermal atoms in the first band can be disregarded. In Fig. 4(d), we present time evolution of the variance $\text{Var}[p_{c,y}]$, focusing on condensed atoms in the second band. We observe similar momentum fluctuation behavior, well-described by the same fitting formula used in Fig. 2(d). The measurements also show that, in the entire course of time evolution, the momentum distribution remains Gaussian, with the variance increasing with time and saturating at long times, leading to an equilibrium distribution. The equilibrium distribution at $t = 940$ ms, obtained from over 3000 repeated measurements, is depicted in Fig. 4(e).

We next present a theoretical analysis, focusing on the condensate COM dynamics in the y -direction which displays sizable momentum fluctuations. Because the condensate COM motion carries a characteristic action much larger than the Planck constant \hbar , the quantum-classical correspondence applies, enabling a classical description of BEC in terms of the phase-space coordinates $(p_{c,y}, y_c)$. Without interactions with incoherent environments, this dynamics is governed by the Hamiltonian $\mathcal{H} = \frac{1}{2}ap_{c,y}^2 + \frac{1}{2}\kappa y_c^2$. The first term is given by the band

dispersion, with the inverse of a being the effective atom mass m^* , and the second term accounts for the residual harmonic potential of the dipole trap and the hexagonal optical lattice, with κ being nearly constant. There is a quartic term $\frac{1}{4}bp_{c,y}^4$ correction to \mathcal{H} , but since in our experiments the motion does not reach out too far from the band minimum at the M point, its effects are neglected. Effects of the interaction between the BEC and its incoherent environments on the BEC dynamics are two-fold. First, the interaction-induced cooling introduces a frictional force. Second, the observed atom loss from the BEC can introduce a random recoil; in addition, via collisions with the condensate, thermal atoms can also introduce random forces. Taking all these into account, we model the condensate COM dynamics by

$$\frac{dy_c}{dt} = \frac{p_{c,y}}{m^*}, \quad \frac{dp_{c,y}}{dt} = -\gamma p_{c,y} - \kappa y_c + \zeta(t). \quad (1)$$

Here $-\gamma p_{c,y}$ and $-\kappa y_c$ are the frictional force (with γ being the friction constant) and the restoring force due to the harmonic potential, respectively. $\zeta(t)$ is a Gaussian white noise of strength Γ that introduces random momentum scattering, whose statistics is completely determined by the autocorrelation: $\text{E}[\zeta(t)\zeta(t')] = \Gamma\delta(t-t')$. One can derive the Fokker-Planck equation from Eq. (1) and find the full phase-space distribution $f(y_c, p_{c,y}; t)$ [33]. Integrating out y_c , we obtain the momentum distribution

$$f(p_{c,y}; t) = \frac{1}{\sqrt{2\pi\text{Var}[p_{c,y}]}} \exp\left(-\frac{(p_{c,y} - \text{E}[p_{c,y}])^2}{2\text{Var}[p_{c,y}]}\right) \quad (2)$$

governed by the instantaneous mean and variance:

$$\text{E}[p_{c,y}] = A_p e^{-\gamma t/2} \sin(\omega_1 t + \phi_p), \quad (3)$$

$$\text{Var}[p_{c,y}] = \frac{\Gamma}{2\gamma} \left(1 - e^{-\gamma t} \left[c_p^2 - \frac{c_p \gamma}{2\omega_1} \sin(2\omega_1 t + \varphi)\right]\right) \quad (4)$$

Here, $\omega_1^2 = \kappa/m^* - \gamma^2/4$, $c_p^2 = \kappa/(m^*\omega_1^2)$, $\tan\varphi = \gamma/(2\omega_1)$, and A_p, ϕ_p depend on the initial $(p_{c,y}, y_c)$, whose explicit forms are given in Ref. [34]. Detailed ab initio microscopic models of the frictional and random forces require more research that is deferred to future work. Here, we show below that Eqs. (2)-(4) suffice to explain the experimental observations quantitatively and understand their physical implications.

As shown in Fig. 2(c) and Fig. 3(a), Eq. (3) well fits the experimental data, and shows that the damped oscillation has angular frequency ω_1 and decay rate $\gamma/2$. In addition, quenching closer to the critical point leads to larger mass m^* , and using the expression of ω_1 we find that this results in the enhancement of the oscillation period, consistent with the experimental data in Fig. 3(a) [34]. Furthermore, because experimentally the sinusoidal oscillation in Eq. (4) can be readily washed out by finite size effects and additionally $c_p^2 \gg c_p \gamma / (2\omega_1)$ for $t \gtrsim \omega_1^{-1}$, Eq. (4) can be simplified to $\text{Var}[p_{c,y}] =$

$\frac{\Gamma}{2\gamma}(1 - c_p^2 e^{-\gamma t})$, which well fits the experimental data, as shown in Figs. 2(d) and 3(b).

Figures 2(b) and 4(e) further show that the full momentum statistics, namely, the Gaussian distribution of Eq. (2) agrees well with the experimental data in the entire course of time evolution. According to Eq. (4), as the time increases, the variance crosses over from a linear growth: $\text{Var}[p_{c,y}] = \Gamma t$ to saturation: $\text{Var}[p_{c,y}] = \Gamma/(2\gamma)$ at the time scale $t_{\text{Th}} = 1/(2\gamma)$. The linear growth suggests that for $t \ll t_{\text{Th}}$ the condensate COM undergoes a diffusive motion in the momentum $p_{c,y}$ space. This has a far-reaching consequence: Similar to stochastic heating in plasma physics [24–26], because a BEC atom has mean kinetic energy $\text{Var}[p_{c,y}]/(2m^*)$, it gets heated up with a constant rate $\Gamma/(2m^*)$ by random momentum scattering. For longer times, the cooling comes into play. According to Eq. (1) the cooling rate is $\gamma \text{Var}[p_{c,y}]/m^*$, which balances the heating rate only if $\text{Var}[p_{c,y}]$ attains the saturation value $\Gamma/(2\gamma)$: This implies that the COM reaches thermal equilibrium at $t \sim t_{\text{Th}}$, and thus t_{Th} gives the thermalization time. Due to Eq. (2) the entire BEC, a ‘classical’ object, displays a Maxwell-Boltzmann distribution at the kinematic temperature

$$T = N_{\text{BEC}} \frac{\text{Var}[p_{c,y}(t \gtrsim t_{\text{Th}})]}{2k_B m^*} = \frac{N_{\text{BEC}} \Gamma}{4k_B \gamma m^*}, \quad (5)$$

with k_B being the Boltzmann constant. Accordingly, for fixed N_{BEC} and T , the enhancement of m^* leads to the enhancement of the saturation value $\Gamma/(2\gamma)$, consistent with the measured temporal profiles of $\text{Var}[p_{c,y}]$ in Fig. 3(b). As detailed in Ref. [34], we can determine $\Gamma/(2\gamma)$ from experimental data and of m^* from calculations. Substituting them and the estimation $N_{\text{BEC}} \simeq 10^3$ into Eq. (5), we obtain $T \simeq 25$ nK for all different cases. This is consistent with an alternative estimation based on the trap depth in the gravity direction [28] and the width of the second band, giving $T \simeq 15$ nK.

The observed temporal profile of $\text{Var}[p_{c,y}]$ resembles dynamical localization [12, 13, 35] and its many-body variant [14–16] in driven cold atomic gases. However, there are conceptual differences. Notably, dynamical localization originates from wave interference and mimics Anderson localization in the momentum space [36, 37], leading to an exponential distribution at equilibrium. In stark contrast, interference plays no role here, and the equilibrium distribution is Maxwell-Boltzmann.

In summary, we have demonstrated that in a BEC interacting with a surrounding thermal cloud and subjected to evaporative cooling induced by atom loss, a sudden quench can lead to an unconventional thermalization process, distinct from the various thermalization mechanisms intensively discussed in previous work [38–41]. Further progress requires a thorough understanding of this interaction on a microscopic level. The present investigations could be extended to systems quenched across the quantum critical point, in order to explore the

interplay between the thermalization process described in the present work and an expected Kibble-Zurek mechanism [42, 43]. Finally, in the present work, the stochastic heating arises from Gaussian white noise. In view of the discovery of quantum turbulence in cold atomic gases [11], it is conceivable that the origin of stochasticity can be more complex leading to richer physics in other non-equilibrium cold atomic systems. This raises the question whether heating by turbulence, which lies at the heart of modern plasma physics [27], has analogies in those systems. Thorough studies of these issues may open a new interdisciplinary research area.

We thank Hui Zhai, Congjun Wu, Shuai Yin, Qi Zhou, Yu Chen, and Masahito Ueda for useful discussions. This work was supported by the National Key R&D Program of China (Grant No. 2022YFA1404103), NSFC (Grants No. 12274196 and No. 12304289), and funds from Guangdong province (Grants No. 2019QN01X087 and No. 2019ZT08X324); C.T. acknowledges support from NSFC (Grants No. 11925507, No. 12475043 and No. 12047503); S.Z. acknowledges support from HK GRF (Grant No. 17306024), CRF (Grants No. C6009-20G and No. C7012-21G), and a RGC Fellowship Award No. HKU RFS2223-7S03; A.H. acknowledges support from the Cluster of Excellence CUI: Advanced Imaging of the Matter of the Deutsche Forschungsgemeinschaft (DFG) - EXC 2056 - project ID 390715994.

* xuzf@sustech.edu.cn

- [1] J. Eisert, M. Friesdorf, and C. Gogolin, “Quantum many-body systems out of equilibrium,” *Nature Physics* **11**, 124–130 (2015).
- [2] Stefan Rotter and Sylvain Gigan, “Light fields in complex media: Mesoscopic scattering meets wave control,” *Rev. Mod. Phys.* **89**, 015005 (2017).
- [3] Elihu Abrahams, *50 Years of Anderson Localization* (World Scientific Publishing Company, 2010).
- [4] Michael P. Zaletel, Mikhail Lukin, Christopher Monroe, Chetan Nayak, Frank Wilczek, and Norman Y. Yao, “Colloquium: Quantum and classical discrete time crystals,” *Rev. Mod. Phys.* **95**, 031001 (2023).
- [5] Toshiya Kinoshita, Trevor Wenger, and David Weiss, “A quantum newton’s cradle,” *Nature* **440**, 900–903 (2006).
- [6] Michael Schreiber, Sean S. Hodgman, Pranjali Bordia, Henrik P. Lüschen, Mark H. Fischer, Ronen Vosk, Ehud Altman, Ulrich Schneider, and Immanuel Bloch, “Observation of many-body localization of interacting fermions in a quasirandom optical lattice,” *Science* **349**, 842–845 (2015).
- [7] Jae-yoon Choi, Sebastian Hild, Johannes Zeiher, Peter Schauß, Antonio Rubio-Abadal, Tarik Yefsah, Vedika Khemani, David A. Huse, Immanuel Bloch, and Christian Gross, “Exploring the many-body localization transition in two dimensions,” *Science* **352**, 1547–1552 (2016).
- [8] Adam M. Kaufman, M. Eric Tai, Alexander Lukin, Matthew Rispoli, Robert Schittko, Philipp M. Preiss,

- and Markus Greiner, “Quantum thermalization through entanglement in an isolated many-body system,” *Science* **353**, 794–800 (2016).
- [9] Logan W. Clark, Lei Feng, and Cheng Chin, “Universal space-time scaling symmetry in the dynamics of bosons across a quantum phase transition,” *Science* **354**, 606–610 (2016).
- [10] E. Nicklas, M. Karl, M. Höfer, A. Johnson, W. Muesel, H. Strobel, J. Tomkovič, T. Gasenzer, and M. K. Oberthaler, “Observation of scaling in the dynamics of a strongly quenched quantum gas,” *Phys. Rev. Lett.* **115**, 245301 (2015).
- [11] Nir Navon, Alexander L. Gaunt, Robert P. Smith, and Zoran Hadzibabic, “Emergence of a turbulent cascade in a quantum gas,” *Nature* **539**, 72–75 (2016).
- [12] F. L. Moore, J. C. Robinson, C. F. Bharucha, Bala Sundaram, and M. G. Raizen, “Atom optics realization of the quantum δ -kicked rotor,” *Phys. Rev. Lett.* **75**, 4598–4601 (1995).
- [13] Julien Chabé, Gabriel Lemarié, Benoît Grémaud, Dominique Delande, Pascal Szriftgiser, and Jean Claude Garreau, “Experimental observation of the anderson metal-insulator transition with atomic matter waves,” *Phys. Rev. Lett.* **101**, 255702 (2008).
- [14] Jun Hui See Toh, Katherine C. McCormick, Xinxin Tang, Ying Su, Xi-Wang Luo, Chuanwei Zhang, and Subhadeep Gupta, “Many-body dynamical delocalization in a kicked one-dimensional ultracold gas,” *Nature Physics* **18**, 1297–1301 (2022).
- [15] Alec Cao, Roshan Sajjad, Hector Mas, Ethan Q. Simmons, Jeremy L. Tanlimco, Eber Nolasco-Martinez, Toshihiko Shimasaki, H. Esat Kondakci, Victor Galitski, and David M. Weld, “Interaction-driven breakdown of dynamical localization in a kicked quantum gas,” *Nature Physics* **18**, 1302–1306 (2022).
- [16] Yanliang Guo, Sudipta Dhar, Ang Yang, Zekai Chen, Hepeng Yao, Milena Horvath, Lei Ying, Manuele Landini, and Hanns-Christoph Nägerl, “Observation of many-body dynamical localization,” (2023), [arXiv:2312.13880](https://arxiv.org/abs/2312.13880) [quant-ph].
- [17] L. D. Landau and E. M. Lifshitz, *Statistical Physics, Part 2: Volume 9* (Pergamon Press; 3rd Edition, 1980).
- [18] Leonid A. Sidorenkov, Meng Khoon Tey, Rudolf Grimm, Yan-Hua Hou, Lev Pitaevskii, and Sandro Stringari, “Second sound and the superfluid fraction in a fermi gas with resonant interactions,” *Nature* **498**, 78–81 (2013).
- [19] Panagiotis Christodoulou, Maciej Galka, Nishant Dogra, Raphael Lopes, Julian Schmitt, and Zoran Hadzibabic, “Observation of first and second sound in a bkt superfluid,” *Nature* **594**, 191–194 (2021).
- [20] Daniel Kai Hoffmann, Vijay Singh, Thomas Paintner, Manuel Jäger, W. Limmer, Ludwig Mathey, and Johannes Hecker Denschlag, “Second sound in the crossover from the bose-einstein condensate to the bardeen-cooper-schrieffer superfluid,” *Nature Communications* **12**, 7074 (2021).
- [21] Timon A. Hilker, Lena H. Dogra, Christoph Eigen, Jake A. P. Glidden, Robert P. Smith, and Zoran Hadzibabic, “First and second sound in a compressible 3d bose fluid,” *Phys. Rev. Lett.* **128**, 223601 (2022).
- [22] Xi Li, Xiang Luo, Shuai Wang, Ke Xie, Xiang-Pei Liu, Hui Hu, Yu-Ao Chen, Xing-Can Yao, and Jian-Wei Pan, “Second sound attenuation near quantum criticality,” *Science* **375**, 528–533 (2022).
- [23] Zhenjie Yan, Parth B. Patel, Biswaroop Mukherjee, Christopher J. Vale, Richard J. Fletcher, and Martin W. Zwierlein, “Thermography of the superfluid transition in a strongly interacting fermi gas,” *Science* **383**, 629–633 (2022).
- [24] Enrico Fermi, “On the origin of the cosmic radiation,” *Phys. Rev.* **75**, 1169–1174 (1949).
- [25] Thomas H. Stix, “Energetic electrons from a beam-plasma overstability,” *Phys. Fluids* **7**, 1960–1979 (1964).
- [26] D. E. Hall and P. A. Sturrock, “diffusion, scattering and acceleration of particles by stochastic electromagnetic fields,” *Phys. Fluids* **10**, 2620–2628 (1967).
- [27] Vahé Petrosian, “Stochastic acceleration by turbulence,” *Space Science Reviews* **173**, 535–556 (2012).
- [28] Xiao-Qiong Wang, Guang-Quan Luo, Jin-Yu Liu, W. Vincent Liu, Andreas Hemmerich, and Zhi-Fang Xu, “Evidence for an atomic chiral superfluid with topological excitations,” *Nature* **596**, 227–231 (2021).
- [29] Jin-Yu Liu, Guang-Quan Luo, Xiao-Qiong Wang, Andreas Hemmerich, and Zhi-Fang Xu, “Experimental realization of a high precision tunable hexagonal optical lattice,” *Optics Express* **30**, 44375 (2022).
- [30] Xiao-Qiong Wang, Guang-Quan Luo, Jin-Yu Liu, Guan-Hua Huang, Zi-Xiang Li, Congjun Wu, Andreas Hemmerich, and Zhi-Fang Xu, “Evidence for quantum stripe ordering in a triangular optical lattice,” *Phys. Rev. Lett.* **131**, 226001 (2023).
- [31] Markus Greiner, Immanuel Bloch, Olaf Mandel, Theodor W. Hänsch, and Tilman Esslinger, “Exploring phase coherence in a 2d lattice of bose-einstein condensates,” *Phys. Rev. Lett.* **87**, 160405 (2001).
- [32] M. Nuske, J. Vargas, M. Hachmann, R. Eichberger, L. Mathey, and A. Hemmerich, “Metastable order protected by destructive many-body interference,” *Phys. Rev. Res.* **2**, 043210 (2020).
- [33] Ming Chen Wang and G. E. Uhlenbeck, “On the theory of the brownian motion ii,” *Rev. Mod. Phys.* **17**, 323–342 (1945).
- [34] For details, see Supplemental Materials.
- [35] G. Casati, B. V. Chirikov, F. M. Izraelev, and Joseph Ford, “Stochastic behavior of a quantum pendulum under a periodic perturbation,” in *Stochastic Behavior in Classical and Quantum Hamiltonian Systems*, Vol. 93, edited by Giulio Casati and Joseph Ford (1979) pp. 334–352.
- [36] Shmuel Fishman, D. R. Grempel, and R. E. Prange, “Chaos, quantum recurrences, and anderson localization,” *Phys. Rev. Lett.* **49**, 509–512 (1982).
- [37] Chushun Tian and Alexander Altland, “Theory of localization and resonance phenomena in the quantum kicked rotor,” *New Journal of Physics* **12**, 043043 (2010).
- [38] Luca D’Alessio, Yariv Kafri, Anatoli Polkovnikov, and Marcos Rigol, “From quantum chaos and eigenstate thermalization to statistical mechanics and thermodynamics,” *Advances in Physics* **65**, 239–362 (2016).
- [39] F. Borgonovi, F.M. Izrailev, L.F. Santos, and V.G. Zelevinsky, “Quantum chaos and thermalization in isolated systems of interacting particles,” *Physics Reports* **626**, 1–58 (2016).
- [40] Rahul Nandkishore and David A. Huse, “Many-body localization and thermalization in quantum statistical mechanics,” *Annual Review of Condensed Matter Physics* **6**, 15–38 (2015).
- [41] Masahito Ueda, “Quantum equilibration, thermalization

and prethermalization in ultracold atoms,” *Nature Reviews Physics* **2**, 669–681 (2020).

- [42] T W B Kibble, “Topology of cosmic domains and strings,” *Journal of Physics A: Mathematical and General* **9**, 1387 (1976).
- [43] W. H. Zurek, “Cosmological experiments in superfluid helium?” *Nature* **317**, 505–508 (1985).

Supplemental Materials

EXPERIMENTAL SYSTEM

Our experiment starts with a ^{87}Rb Bose-Einstein condensate consisting of typically 6.8×10^4 atoms in the $|F = 1, m_F = -1\rangle$ state. The condensate is prepared in an oblate optical dipole trap with trapping frequencies $\{\omega_x, \omega_y, \omega_z\} = 2\pi \times \{26.4, 26.5, 69.5\}$ Hz. Atoms are subsequently loaded into the deformed hexagonal lattice, which is realized by superimposing two sets of triangular optical lattices with lattice sites denoted as A and B respectively. They are created by three running-wave laser beams linearly polarized parallel to the z -axis and intersecting at an angle of 120° in the xy -plane. Each laser beam comprises two frequency components of ν_1 and ν_2 with their difference defined as $\Delta\nu = \nu_1 - \nu_2$. Both wavelengths are $\lambda \simeq 1064$ nm. The lattice potential is thus given by

$$V(\mathbf{r}) = -V_A \left[3 + 2 \sum_j \cos(\mathbf{b}_j \cdot \mathbf{r}) \right] - V_B \left[3 + 2 \sum_j \cos(\mathbf{b}_j \cdot \mathbf{r} - \Delta\eta_j) \right]. \quad (\text{S1})$$

Here, the vectors \mathbf{b}_j are defined as $\mathbf{b}_1 = \mathbf{k}_1 - \mathbf{k}_2$, $\mathbf{b}_2 = \mathbf{k}_2 - \mathbf{k}_3$, and $\mathbf{b}_3 = \mathbf{k}_3 - \mathbf{k}_1$ with the wave vectors $\mathbf{k}_1 = k_L(-\sqrt{3}/2, 1/2)$, $\mathbf{k}_2 = k_L(\sqrt{3}/2, 1/2)$, and $\mathbf{k}_3 = k_L(0, -1)$, where $k_L = 2\pi/\lambda$ and $j = 1, 2, 3$. $\Delta\eta_j = 2\pi\Delta\nu\Delta L_j/c$ determine the difference of the centers of the two triangular lattices. Experimentally, we choose $(\Delta L_1, \Delta L_2, \Delta L_3) \simeq (-6.12, 3.06, 3.06)$ cm by changing the optical paths of the laser beams forming the triangular lattices. Since $\Delta L_2 = \Delta L_3$, tuning $\Delta\nu$ thus changes the separation of the centers of the two triangular lattices along the x -axis. In the case of $\Delta\nu = 3.263$ GHz, $V(\mathbf{r})$ becomes a regular hexagonal lattice. For other cases, a deformed hexagonal lattice is realized.

STATE PREPARATION AND DETECTION

Initially, atoms are loaded into the lowest s -orbital of the deformed hexagonal optical lattice with $\Delta\nu = 3.19$ GHz and $(V_A, V_B) = (7.99, 5.16) E_R$, where $E_R = \hbar^2/2m\lambda^2$ is the recoil energy. By quickly changing (V_A, V_B) to $(7.32, 7.93) E_R$ in 0.1 ms, the atoms are transferred to the second Bloch band of the lattice and, via active cooling, are later recondensed in the minimum of

the second band, located at the M point. In order to ensure efficient and continuous cooling of the atoms, the intensity of the optical dipole trap is linearly reduced to a certain value within 15 ms, and the final value is carefully optimized to provide a scattering channel for the thermal atoms to escape from the trap along the direction of gravity via collisions. After a holding time of 105 ms, we suddenly change $\Delta\nu$ from 3.19 GHz to a value close to, but not beyond the critical point of the effectively ferromagnetic quantum phase transition. This operation is completed within 0.5 ms. In the following dynamics, we observe the center-of-mass oscillation and fluctuations of the condensate in momentum space over time, centered around the energy minimum of the second Bloch band, using time-of-flight spectroscopy or a band mapping technique.

BAND DISPERSION ENGINEERING

In our experiment, we consider a situation with different final lattice depths among the A and B sites with $(V_A, V_B) = (7.32, 7.93) E_R$. When the atoms are transferred into the second Bloch band, they mainly populate the shallow s -orbitals of the A sites. This leads to an extremely long lifetime. Via tuning $\Delta\nu$, we can significantly change the band dispersion along the y direction, which is shown in Fig. 1(b). In this case, the critical point is estimated to be located around $\Delta\nu_C = 3.235$ GHz. To characterize the band dispersion along the y direction, we fit it with $\mathcal{E} = \mathcal{E}_0 + \frac{1}{2}a p_y^2 + \frac{1}{4}b p_y^4$ along the line connecting the K_1 and K_2 points. When $\Delta\nu < \Delta\nu_C$, $a > 0$, while in the opposite case, the band structure shows a double-well dispersion with $a < 0$. Focusing on the case with $\Delta\nu < \Delta\nu_C$, we numerically calculate the corresponding parameter of a to evaluate the effective mass along the y direction denoted as $m^* = 1/a$. Details are shown in Fig. S1(a). We approximately choose the overall trapping potential via including the contribution from the dipole trap and the optical lattice along the y -direction to be $2\pi \times 50$ Hz. This enables us to roughly estimate the oscillation period $2\pi/\omega_0$, where $\omega_0 \equiv \sqrt{\kappa/m^*}$. Details are shown in Fig. S1(b). Furthermore, using the value of γ from experimental data fitting, we calculate ω_1 shown in Fig. S1(c). The obtained oscillation period $2\pi/\omega_1$ is consistent with experimentally observed oscillation period for the mean value of momentum along the y direction shown in Fig. 3(c).

RANDOM FORCE INDUCED BY ATOM LOSS

There are different sources giving rise to the random force. Here we point out a mechanism, which is highly relevant to our experiments but yet remains largely unexplored in the literature. That is, atoms can escape

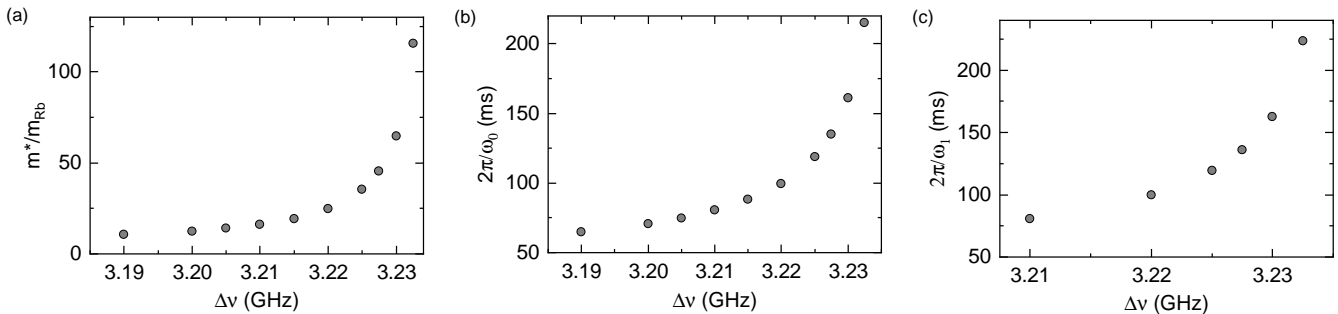


FIG. S1. (a) The effective mass m^* for the second Bloch band along the y -direction is plotted versus the frequency difference $\Delta\nu$ with $(V_A, V_B) = (7.32, 7.93) E_R$. (b) The estimated oscillation period $2\pi/\omega_0$ with the trapping frequency approximately chosen as $2\pi \times 50$ Hz. (c) The oscillation period $2\pi/\omega_1$. Here $\omega_1^2 = \omega_0^2 - \gamma^2/4$. The corresponding values of γ are determined from experimental data fitting.

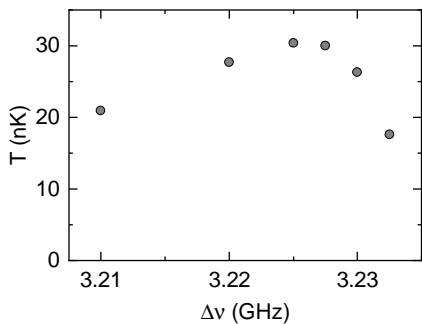


FIG. S2. The estimated temperature for the thermal bath is plotted versus the frequency difference $\Delta\nu$.

from the condensate, and introduce a random recoil. As observed in experiments, the atoms mostly condense at a single quasi-momentum. So a condensed atom carries in y -direction a momentum $p_{c,y}$ on the average. Suppose that at time t the BEC consists of $N(t)$ atoms. Then it carries an instantaneous total momentum: $N(t)p_{c,y}(t)$. Let an small amount of atoms, $N_L(t) \equiv N(t) - N(t + \delta t)$, be lost from BEC during a small time interval δt , each of which carries a momentum $p_L(t) \equiv p_{c,y}(t) + \xi(t)$. Here $\xi(t)$ is random and introduces a random recoil to the condensate. Since the total momentum is conserved, we have

$$\begin{aligned} & N(t + \delta t)p_{c,y}(t + \delta t) + N_L(t)p_L(t) \\ &= N(t)(p_{c,y}(t) - \kappa y_c \delta t), \end{aligned} \quad (\text{S2})$$

where y_c denotes the mean position of a condensed atom in the y -direction, and $-N(t)\kappa y_c \delta t$ is the total momentum input by the external harmonic trap. Setting $\delta t \rightarrow 0$ we obtain

$$\frac{dp_{c,y}}{dt} = -\kappa y_c + \frac{d \ln N}{dt} \xi. \quad (\text{S3})$$

This equation is difficult to solve because the random recoil $\xi(t)$ is coupled to the atom loss, i.e. $\frac{d \ln N}{dt}$. To overcome this difficulty we instead treat the second term as

a whole as a random force $\zeta(t) \equiv \frac{d \ln N}{dt} \xi(t)$. So Eq. (S3) is simplified to

$$\frac{dp_{c,y}}{dt} = -\kappa y_c + \zeta(t). \quad (\text{S4})$$

With the friction force $\gamma p_{c,y}$ being included, we then obtain Eq. (1) of the main text. As said above, there are other sources of random force such as thermal atoms. They add together, however, and thus do not change the form of this equation of motion.

FRICTION FORCE DUE TO COOLING

In our system there is a cooling mechanism, which enables transferring kinetic energy from the xy plane to the z -axis via collisions. This opens an efficient channel for evaporation of atoms with high kinetic energy stored in the z -direction aided by gravity. This active cooling may serve as an origin for the friction force applied to the BEC, accounted by the first term in Eq. (1) of the main text.

MOMENTUM DISTRIBUTION

For simplicity we assume that ζ is a Gaussian white noise with $\langle \zeta(t) \rangle = 0$ and $\langle \zeta(t)\zeta(t') \rangle = \Gamma \delta(t-t')$. We can derive a Fokker-Planck equation for the Langevin model described by Eq. (1) in the main text, from which we find the instantaneous phase-space distribution function in the phase space coordinates $(y_c, p_{c,y})$, read

$$f(y_c, p_{c,y}; t) = e^{t\mathcal{L}_{\text{FP}}} \delta(y_c - y_0) \delta(p_{c,y} - p_0), \quad (\text{S5})$$

where the operator

$$\mathcal{L}_{\text{FP}} = -\frac{p_{c,y}}{m^*} \partial_{y_c} + \partial_{p_{c,y}} (\gamma p_{c,y} + \omega_0^2 y_c) + \frac{\Gamma}{2} \partial_{p_{c,y}}^2, \quad (\text{S6})$$

and (p_0, y_0) are the initial coordinates. Define a two-component complex vector $\mathbf{z} = (z_1, z_2)^T$, whose components are $z_{1,2} = p_{c,y}/m^* + a_{1,2}y_c$, with $a_{1,2} = \gamma/2 \pm i\omega_1$. Then we can write Eq. (S5) explicitly, which is

$$f(y_c, p_{c,y}; t) = -2i\omega_1 \int \frac{d\boldsymbol{\eta}}{(2\pi)^2} e^{i\boldsymbol{\eta}^T(\mathbf{z}-\mathbf{z}_0(t)) - \frac{1}{2}\boldsymbol{\eta}^T A(t)\boldsymbol{\eta}}. \quad (\text{S7})$$

Here

$$\mathbf{z}_0(t) = \begin{pmatrix} (p_0/m^* + a_1 y_0)e^{-a_2 t} \\ (p_0/m^* + a_2 y_0)e^{-a_1 t} \end{pmatrix}, \quad (\text{S8})$$

and

$$A(t) = \frac{\Gamma}{\gamma m^{*2}} \begin{pmatrix} \frac{1-e^{-(1-is_p)\gamma t}}{1-is_p} & 1-e^{-\gamma t} \\ 1-e^{-\gamma t} & \frac{1-e^{-(1+is_p)\gamma t}}{1+is_p} \end{pmatrix}, \quad (\text{S9})$$

with $s_p = 2\omega_1/\gamma$, and $\boldsymbol{\eta} = (\eta_1, \eta_2)^T$.

The expression (S7) allows us to perform the integral over y_c and find the momentum distribution $f(p_{c,y}; t)$. The result is

$$f(p_{c,y}; t) = \int \frac{d\eta}{2\pi} e^{i\eta[p_{c,y} - A_p e^{-\frac{\gamma t}{2}} \sin(\omega_1 t + \phi_p)]} \times e^{-\frac{\Gamma}{4\gamma} \{1 - e^{-\gamma t} [c_p^2 - \frac{c_p}{s_p} \sin(2\omega_1 t + \varphi)]\} \eta^2}, \quad (\text{S10})$$

where $A_p = \sqrt{(\frac{1}{2}p_0\gamma + \kappa y_0)^2/\omega_1^2 + p_0^2}$, $\tan(\phi_p) = -p_0\omega_1/(\frac{1}{2}p_0\gamma + \kappa y_0)$, $\omega_1^2 = \omega_0^2 - \gamma^2/4$, $c_p = \omega_0/\omega_1$, and $\tan(\varphi) = 1/s_p$. Integrating out η , we obtain Eqs. (2)-(4) in the main text.